GEODESY AND CARTOGRAPHY
Vol. 70, no. 2, article no. e08, 2021

DOI: https://doi.org/10.24425/gac.2021.136683

Original paper

Part of Topical collection:
"Geodetic techniques in observations of mining deformations and induced seismicity – EPOS-PL"

Cross-comparison of meteorological parameters and ZTD observations supplied by microwave radiometers, radiosondes, and GNSS services

Estera Trzcina*, Damian Tondaś, Witold Rohm

Wroclaw University of Environmental and Life Science, Wroclaw, Poland
e-mail: estera.trzcina@upwr.edu.pl; ORCID: http://orcid.org/0000-0003-0068-6543
e-mail: damian.tondas@upwr.edu.pl; ORCID: http://orcid.org/0000-0001-7922-4469
e-mail: witold.rohm@upwr.edu.pl; ORCID: http://orcid.org/0000-0002-2082-6366

*Corresponding author: Estera Trzcina, e-mail: estera.trzcina@upwr.edu.pl

Received: 2021-07-05 / Accepted: 2021-09-29

Abstract: Water vapour radiometers (WVR) provide information about temperature and humidity in the troposphere, with high temporal resolution when compared to the radiosonde (RS) observations. This technique can provide an additional reference data source for the zenith tropospheric delay (ZTD) estimated with the use of the Global Navigation Satellite System (GNSS). In this work, the accuracy of two newly installed radiometers was examined by comparison with RS observations, in terms of temperature (T), absolute humidity (AH), and relative humidity (RH), as well as for the ZTD. The impact of cloud covering and heavy precipitation events on the quality of WVR measurements was investigated. Also, the WVR data were compared to the GNSS ZTD estimates. The experiment was performed for 17 months during 2020 and 2021. The results show agreement between RS and WVR data at the level of 2°C in T and 1 g m^{-3} in AH, whereas for RH larger discrepancies were noticed (standard deviation equal to 21%). Heavy precipitation increases WVR measurement errors of all meteorological parameters. In terms of ZTD, the comparison of WVR and RS techniques results in bias equal to –0.4 m and a standard deviation of 7.4 mm. The largest discrepancies of ZTD were noticed during the summer period. The comparison between the GNSS and WVR gives similar results as the comparison between the GNSS and RS (standard deviation 7.0–9.0 mm).

Keywords: water vapour radiometers, zenith tropospheric delay, GNSS meteorology

1. Introduction

Atmospheric water vapour is a principal contributor to the climate changes, as well as the main factor shaping weather conditions (Ingram, 2010; Van Baelen et al., 2011). Information about its spatio-temporal distribution is a crucial part of climate science and weather prediction processes (Jacob, 2001; Ferreira et al., 2016; Zhao et al., 2019b). However, a complex circulation and high temporal variability of water vapour content in the atmosphere make it very demanding to observe (Bengtsson, 2010; Buehler et al., 2012).

The most common technique of tropospheric water vapour measurements are radiosonde (RS) observations. This method is widely used since the 1950s and delivers reliable information about the tropospheric state (Miloshevich et al., 2004). The main limitation of the RS technique is its high cost, leading to a low resolution in time and space (12 hours, about 250 km in Europe) which prevents monitoring of rapid changes in atmospheric humidity. Starting from the 1990s, Global Navigation Satellite System (GNSS) observations have been used to estimate water vapour's distribution in the troposphere (Bevis et al., 1994; Guerova et al., 2016). In contrast to the RS measurements, the GNSS estimations of a tropospheric state can be conducted without the need for additional expensive equipment, with a resolution of 1 hour or less (Karabatić et al., 2011; Tondaś et al., 2020). A main product of the GNSS meteorology is a zenith tropospheric delay (ZTD) containing information about the GNSS signals' delay caused by tropospheric refraction (Böhm and Schuh, 2013). Also, precipitable water vapour (PWV) can be estimated using additional information about pressure and temperature at the measurement's site (Karabatić et al., 2011; Liang et al., 2015). Both quantities are successfully assimilated into experimental and operational Numerical Weather Prediction (NWP) models (Boniface et al., 2009; Bennitt and Jupp, 2012; Mahfouf et al., 2015; Rohm et al., 2019). Also, attempts to use GNSS-derived humidity information in a climate monitoring were made (Gradinarsky et al., 2002; Morland et al., 2009; Vey et al., 2010). First results of assimilation of GNSS-derived slant tropospheric delays (STD) (Bauer et al., 2011; Zus et al., 2011) as well as GNSS troposphere tomography products (Möller et al., 2015; Hanna et al., 2019; Trzcina and Rohm, 2019; Trzcina et al., 2020) show a high potential of the GNSS tropospheric humidity estimations for the NWP models. However, well-established quality control of the assimilated observations, as well as their proper weighting, is crucial in this process (Trzcina et al., 2020).

According to the EIG EUMETNET GNSS Water Vapour Programme (E-GVAP-II) Product Requirements Document (Offiler, 2010), verification of the GNSS-derived humidity products can be conducted using radiosondes and water vapour radiometers (WVR) observations. The former is a very commonly used and reliable validation data source for the GNSS meteorology products (Bock et al., 2016; Pacione et al., 2017; Zhao et al., 2019a). However, a spatial and temporal resolution of the radiosonde measurements is the biggest limitation in the verification of the much denser and more frequently acquired GNSS products. The microwave radiometers are used in verification of the GNSS humidity estimates with a standard resolution of 1 hour (Lu et al., 2016); first attempts of a high temporal resolution comparisons (5 minutes) have been made

by Ning and Elgered, (2021). The studies show agreement between PWV measured by WVR and GNSS estimates at the level of 1-4 mm (Ohtani and Naito, 2000; Liou et al., 2001; Dai et al., 2002). In the experiment by Wang and Liu (2019) a bias between WVR and GNSS was detected, equal to –2.7 mm for PWV. The main limitation of the WVR technique is its sensitivity to the rainy conditions, when the measurement error increases (Shangguan et al., 2015). Comparing the two validation techniques, the studies show the better agreement of PWV between WVR and GNSS than between radiosondes and GNSS (Guerova et al., 2005; Liu et al., 2005; Van Baelen et al., 2005; Wang and Liu, 2019). In Poland, the GNSS estimates of the tropospheric state are usually validated against radiosonde observations, as they are a reliable and easily accessible meteorological data source (Dymarska et al., 2017; Trzcina and Rohm, 2019; Tondaś et al., 2020). Water vapour radiometers can provide additional information about humidity in the troposphere, with time resolution more suitable for the GNSS measurements' verification. This is especially beneficial for GNSS tomography retrievals, which are provided with high temporal resolution (Sá et al., 2021) – up to 5 minutes, but cannot be validated with other techniques (e.g. radiosonde measurements). As a consequence, usage of microwave radiometers as an additional data source in validation of the GNSS tropospheric products can potentially lead to a better quality of the GNSS data for meteorology, e.g. by additional filtration process or improved errors' assignment in assimilation into the NWP models.

This study aims to verify an agreement between measurements of two newly installed microwave radiometers against standard meteorological data sources, i.e. radiosonde observations and numerical weather prediction model, in terms of temperature and humidity. Also, GNSS estimations of zenith tropospheric delay (ZTD) were validated against WVR and RS observations. Data used in the experiment are described in Section 2. The methodology of the study is presented in Section 3. Sections 4 and 5 show results of the performed comparisons, for the meteorological parameters and ZTD values respectively. The main conclusions are presented in Section 6.

2. Data sets

The study was conducted in two locations in Poland, i.e. Wrocław and Borowa Góra (Fig. 1). In both cases, three types of research equipment were used: microwave radiometers, radiosonde meteorological stations, and GNSS stations. In Wrocław, microwave radiometer 003 0138 and GNSS station WROC are installed on roof of the building of the Institute of Geodesy and Geoinformatics (IGiG) at the Wrocław University of Environmental and Life Sciences, a distance between the two instruments is not larger than 5 m. Radiosonde station 12425 is located on the premises of the Institute of Meteorology and Water Management (IMGW), 10 km from IGiG. Microwave radiometer 003 134 and GNSS station BOGI are located in Geodetic-Geophysical Observatory "Borowa Góra" of Institute of Geodesy and Cartography and the distance between them is not larger than 100 m, whereas the radiosonde station 12374 is about 12 km away from these instruments.

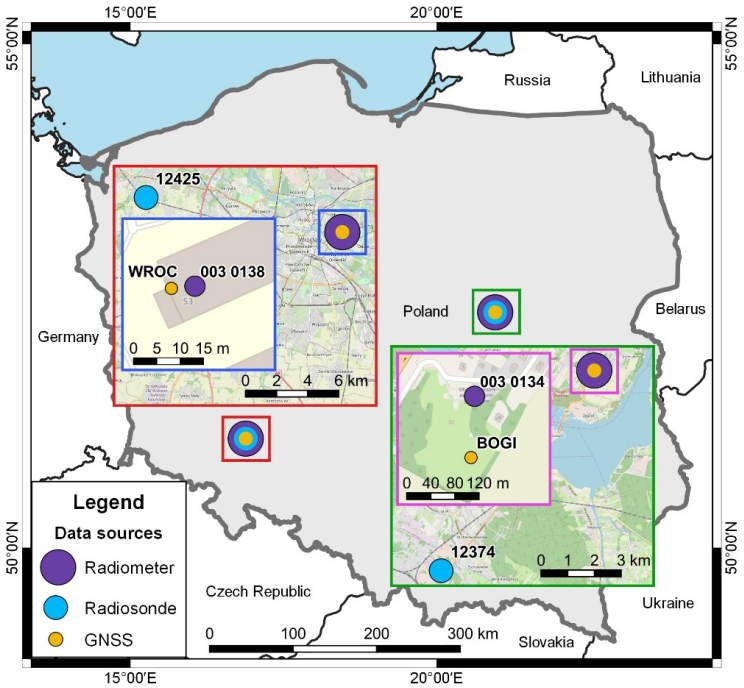

Fig. 1. Location of the research equipment used in two spots (Wrocław, Borowa Góra); two sets of equipment were used, each consisting of one microwave radiometer (003 0138 in Wrocław, 003 0134 in Borowa Góra), one radiosonde station (12425 in Wrocław, 12374 in Borowa Góra), and one GNSS station (WROC in Wrocław, BOGI in Borowa Góra)

2.1. Microwave radiometers

In this research, two RPG-HATPRO-G5 (Humidity And Temperature PROfiler, single-polarization) microwave radiometers manufactured by RPG (Radiometer Physics GmbH, Germany) were used (RPG, 2017). The measurement principles of the microwave radiometers are based on passive observations of atmospheric components' thermal emission in the microwave spectral range (Ferraro et al., 1998). The observations of radiances are converted into brightness temperatures whose values and variations at different frequencies are correlated to selected atmosphere parameters (Ulaby et al., 1986). Further, the neural network algorithms are used to retrieve information about the meteorological variables (Churnside et al., 1994; Frate and Schiavon, 1998; Solheim et al., 1998). In the instruments from the HATPRO-G5 series, standard feed-forward neural network (Jung et al., 1998) is used, where the cost function is minimized employing the Davidon–Fletcher–Powell algorithm. The process is based on a data set of atmospheric profiles of temperature, pressure, and humidity measured by radiosondes. The RPG-HATPRO-G5 instruments measure at 14 channels parallelly: 6 channels along the water vapour absorption line centred at 22.235 GHz with 1 additional window channel at 31.40 GHz (used for humidity profiles retrieval), 7 channels along the oxygen

absorption complex around 60 GHz (used for temperature profiles retrieval). All available channels' centre frequencies together with their band widths are given in Table 1. Temperature profiling is available in zenith observation mode (continuous observation in the vertical direction) and boundary layer mode (scanning the atmosphere in elevation, using channels above 54 GHz with the highest absorption below 1 km altitude). In this study, a combination of the two modes was used. In the case of absolute humidity, only a zenith mode is available, as the atmosphere is transparent at the water vapour channel frequencies around 22 GHz (no saturation of the brightness temperatures occurs). Relative humidity values are obtained using a dedicated retrieval which derives values directly from the radiometer's measurement.

Table 1. RPG-HATPRO-G5 channel centre frequencies (fc) and corresponding bandwidths (b)

fc [GHz]	22.24	23.04	23.84	25.44	26.24	27.84	31.4	51.26	52.28	53.86	54.94	56.66	57.3	58
b [MHz]	230	230	230	230	230	230	230	230	230	230	230	600	1000	2000

The radiometers used in this study enable to permanently monitor weather conditions with a one-second recording interval, parallelly in all frequency channels. An application of infrared radiometers enables detection of cloud covering and determination of the height cloud base. The microwave radiometers are equipped with Vaisala WXT530 weather stations providing surface measurements of pressure, temperature, relative humidity, wind speed and direction, and total rainfall rate. The instruments' software provides information about integrated tropospheric quantities, including integrated water vapour content (IWV), liquid water path (LWP), zenith tropospheric delay divided into hydrostatic (zenith hydrostatic delay, ZHD) and non-hydrostatic (zenith wet delay, ZWD) parts. Moreover, the radiometer located in Wrocław is equipped with an azimuth positioner, which allows rotating the whole instrument from 0° to 360° horizontally and vertically from 0° to 90°. The radiometer in Wrocław became fully operational on January 11, 2020, while the instrument located in Borowa Góra started data registration on February 7, 2020.

2.2. Meteorological radiosondes

Radiosonde data (RS) were derived from the NOAA/ESLR Radiosonde Database managed by the Earth System Research Laboratory (ESLR) of the National Oceanic and Atmospheric Administration (NOAA: www.esrl.noaa. gov). Observations from two radiosondes were used, i.e., 12374 (for the location of Borowa Góra) and 12425 (for Wrocław). The radiosonde data are available twice a day, at 00:00 and 12:00 UTC. The measurements of temperature, dew point temperature, and wind speed components are provided for the pressure levels in a range of 1000–10 hPa. There are 14 mandatory levels, but depending on the meteorological conditions, more data can be derived (usually

for 30–40 levels). According to the E-GVAP-II Product Requirements Document (Offiler, 2010), radiosonde stations are one of the standard data sources used as a reference in the measurement of the state of the troposphere.

2.3. WRF-ARW model

The Weather Research and Forecasting-Advanced Research (WRF-ARW) model is a numerical weather prediction system designed for the simulation of multiscale, spatial, and temporal atmosphere flows (Skamarock et al., 2008). The system was developed and maintained by the National Center for Atmospheric Research (NCAR) Mesoscale and Microscale Meteorology Laboratory. In this research, the WRF model run by the Department of Climatology and Atmosphere Protection of the University of Wrocław was used (Kryza et al., 2013). The forecasts are produced using WRF-ARW version 3.6.1, with the initial and boundary conditions derived from the Global Forecast System model provided by the National Center for Environmental Prediction (NCEP GFS). The model is run in a near real-time and the forecasts are available every 6 hours (at 00:00, 06:00, 12:00, 18:00 UTC), providing data for the next 48 hours, for the area of Central Europe. Two domains are used, i.e. the general with 12 km resolution and the nested with 4 km resolution. In this research, data from the inner domain were used, where the convection is resolved explicitly.

2.4. GNSS data processing

To determine the ZTD parameter using the GNSS technique, three calculating services were used in the study: ultra-fast Near Real-Time (NRT) system (Tondaś et al., 2020), post-processing (PP) final service, and a combination of European GPS troposphere solutions (Pacione et al., 2011). The first two services were developed by the WUELS processing centre at the Wroclaw University of Environmental and Life Sciences, Poland. The third data source was provided by the EPN Analysis Centre CGS (Italian Space Agency, Centro di Geodesia Spaziale, Matera, Italy) as a combination of results from the centres included in the E-GVAP programme (http://egvap.dmi.dk/).

The ultra-fast NRT processing of GNSS data allows obtaining troposphere parameters and coordinates with a 15-minute estimation latency. This service was implemented through an upgrade of the computational procedures used by Bernese GNSS Software v.5.2 (Dach et al., 2015) concerning the standard hourly NRT processing. The post-processing technique involves the final GNSS products and allows them to achieve the highest level of ZTD accuracy. The main aim of creating the PP system was to establish a reference data source to ultra-fast NRT results. The EPN AC products are derived from an epoch-wise combination of the individual Local Analysis Centre (LAC) solutions with a sampling rate of 1 hour based on weighted means from at least 3 solutions. Most of the 16 LACs providing the solutions for EPN combination use them for daily solutions. Table 2 shows the most frequently applied settings in processing strategies.

The three computing GNSS services use different methods and parameters to determine the zenith delay. The most crucial differences between calculation scenarios are: the latency of receiving results, the interval of estimation, and the sources of reference products and a priori data. A detailed comparison of the performance of the GNSS services is presented in Table 2.

Table 2. The ultra-fast Near Real-Time (NRT), post-processing final (PP), and EPN Analysis Centre ZTD combination (EPN final) processing parameters

Processing parameters	NRT	PP	EPN final
GNSS product type	IGS ultra-rapid	CODE final	CODE ultra-rapid
latency of results	15 min	2 weeks	1–2 month
interval of ZTD estimation	15 min	30 min	1 h
observation window	6 h	24 h	24 h
GNSS observation system	GPS, GLONASS	GPS, GLONASS, Galileo	GPS, GLONASS
type of solution	double-differenced	double-differenced	double-differenced
ZTD a priori and MF	VMF1-FC	VMF1	VMF1-FC
ZTD horizontal gradients	Chen and Herring	Chen and Herring	Chen and Herring

3. Methodology

The study was performed in two steps (Fig. 2). First, meteorological parameters, i.e. temperature (T), absolute humidity (AH), and relative humidity (RH), were compared between three different data sources: microwave radiometers (WVR), radiosonde measurements (RS), and the WRF model. As a result, the quality of the microwave radiome-

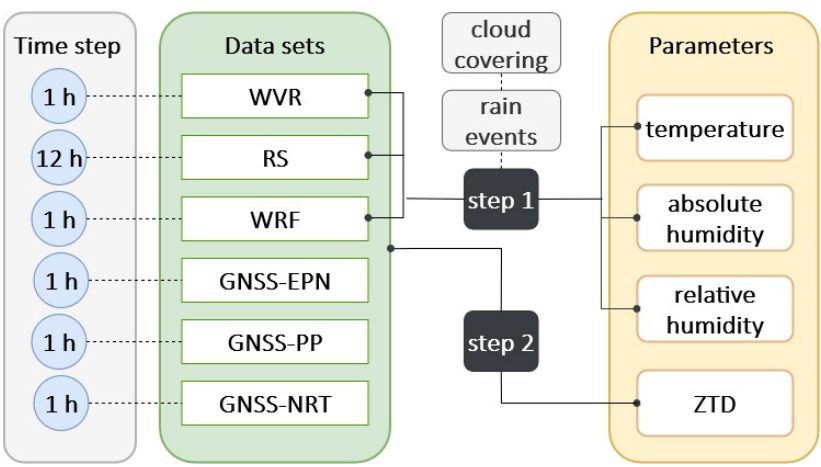

Fig. 2. The scheme of the experiment; the used data sets (green) and compared parameters (yellow) are presented, together with the additional settings (grey)

ter's data was assessed in terms of bias and standard deviation. Also, the impact of cloud covering and rain events on the radiometers' measurements were investigated. In step 2, values of Zenith Tropospheric Delay (ZTD) were obtained from the six data sets and compared to each other. In compliance with the E-GVAP-II Product Requirements Document (Offiler, 2010), the microwave radiometers' and radiosondes' measurements were used as a reference for calculation of the statistics (bias, standard deviation) of ZTD from the WRF model and 3 GNSS solutions (EPN, PP, NRT). The experiment was performed for the period from January 1, 2020, to May 31, 2021. The Time step was 12 hours for radiosonde measurements and 1 hour for the other data sets. The observations were not interpolated in time.

3.1. Step 1 – meteorological parameters comparison

In case of microwave radiometers, profiles of temperature, absolute humidity, and relative humidity in troposphere are available directly from the RPG-HATPRO-G5 software with time resolution of 1 minute, for 93 levels, starting from the ground up to 10 km. Radiosonde measurements do not provide all of these parameters directly, as sensors on board provide information about temperature, dew point temperature, and wind speed components. Therefore, additional calculations of AH and RH were needed. Absolute humidity AH, i.e. absolute amount of water vapor in air, expressed in g m^{-3}, was calculated using a formula given by Böhm and Schuh (2013):

$$AH = \frac{0.794}{1+\alpha \cdot t} \cdot e \tag{1}$$

where t is temperature [°C], α is a constant equal to 0.003661, e is a water vapour partial pressure [hPa] calculated using Magnus formula (Böhm and Schuh, 2013):

$$e = 6.1078 \cdot \exp\left(\frac{17.1 \cdot t_d}{235 + t_d}\right) \tag{2}$$

where t_d is a dew point temperature [°C]. Relative humidity RH [%] was calculated as a ratio of water vapor partial pressure e to the saturated water vapour E [hPa] (Kleijer, 2004):

$$RH = \frac{e}{E} \tag{3}$$

where E was calculated using Magnus formula (Eq. (2)) with temperature t instead of dew point temperature t_d. In the WRF, temperature values are available directly from the model; AH and RH were calculated using Eq. (1) and Eq. (3) respectively, where e was calculated from the model's variables of total air pressure p [hPa] and water vapour mixing ratio q:

$$e = \frac{p \cdot q}{0.62197 + 0.37803 \cdot q} \tag{4}$$

As the three data sets used in step 1 have different vertical resolutions, all of the data were linearly interpolated to the mandatory pressure levels of the RS measurements,

i.e. 1000, 925, 850, 700, 500, 400, 300, 250, 200, 150, 100, 70, 50, and 10 hPa. No extrapolation was applied, thus usually 7 of the most upper layers were omitted (as the WVR measurements are conducted up to 10 km). In the case of the WRF model, two locations were considered separately, for the radiometer (WVR-WRF comparison) and for the radiosonde station (WRF-RS comparison).

The three meteorological parameters (T, AH, RH) were compared between three data sets (WVR, RS, WRF) and the statistics of bias and standard deviation were calculated. The former was calculated as a mean value of the differences between two data sets; the latter is a standard deviation of these differences. The impact of the cloud coverage and rain events was checked based on the values of cloud base height (CBH) measured by the microwave radiometers and the rain flag values given by the radiometer's software to each measurement. The CBH is measured with a time step of 1 minute and is given in meters. Epochs, where the radiometer detected CBH for the levels up to 10 km, were treated as the epochs with the cloud covering; otherwise, the clear-sky conditions were assumed. The epochs with rain are those where the radiometer's rain flag was set to 1, otherwise, no rain was assumed. The impact of these meteorological conditions was investigated by calculation of the statistics separately for the rainy and not rainy epochs. Also, the impact of the CBH on the T, AH, and RH profiles was checked for each measurement epoch.

3.2. Step 2 – Zenith Tropospheric Delay comparison

ZTD values were calculated from the meteorological data sets (RS, WRF) as a sum of the Zenith Hydrostatic Delays (ZHD) and Zenith Wet Delays (ZWD):

$$ZTD = ZHD + ZWD \tag{5}$$

The hydrostatic part ZHD [m] was calculated using Saastamoinen formula (Kleijer, 2004):

$$ZHD = \frac{0.0022768 \cdot p}{1 - 0.00266 \cdot \cos(2\varphi) - 0.00000028 \cdot H} \tag{6}$$

where p is a total air pressure [hPa], φ denotes the location's latitude, and H is the normal height [m]. The wet part of the delay (ZWD [m]) was calculated by integration of wet refractivity values N_w along the vertical profiles of the troposphere (Wilgan et al., 2015):

$$ZWD = 10^{-6} \cdot \sum_{i=1}^{k} \frac{N_{w,i+1} + N_{w,i}}{2} \cdot \Delta s_i \tag{7}$$

where $N_{w,i}$ is a wet refractivity for the i-th level [ppm], Δs_i is a distance between $(i+1)$-th and i-th measurement's or model's level [m], k is the number of vertical spaces between measurements' or model's layers. N_w was derived using the values of temperature T [K] and water vapour partial pressure e [hPa] with the formula (Kleijer, 2004):

$$N_w = \left(k_2' \frac{e}{T} + k_3 \frac{e}{T^2}\right) Z_w^{-1} \tag{8}$$

where Z_w^{-1} is the inverse compressibility factor of the wet air, k_2' and k_3 are empirical constants, equal to 17 K hPa^{-1} and $3.776 \cdot 10^5$ K hPa^{-1} respectively (Thayer, 1974). ZTD values of the WRF model were extracted separately for GNSS and the radiosonde stations' locations. In the case of the microwave radiometer and the GNSS data sets, the ZTD values were available without further computation.

In the ZTD comparison process, first, the microwave radiometers' results of the ZTD measurement were validated against the radiosonde data to assess the quality of the WVR measurement technique. Next, the results of the WRF model and the four GNSS solutions were validated against the radiosondes', and radiometers' data which were treated as a reference. The statistics of bias (mean of the differences) and standard deviations were calculated to check the consistency between the solutions and the reference data sets.

4. Cross-comparison of the meteorological parameters

4.1. Meteorological parameters – comparison between radiometers and radiosondes

The vertical profiles of T, AH, and RH measured by the microwave radiometers were compared to the radiosonde data for the entire period, with a time step of 12 hours. Statistics of the discrepancies between RS and WVR measurements of temperature and humidity parameters are presented in Table 3. A negative bias of temperature is noticed for Wrocław and Borowa Góra with values of –0.41°C and –0.17°C respectively. The humidity in the troposphere seems to be slightly overestimated by the radiometers' measurements, when compared to the radiosondes, since the bias is positive for both AH and RH in the two locations (0.09 g m^{-3} and 0.21 g m^{-3} in terms of AH, 3.24% and 3.60% in terms of RH). Standard deviations of temperature measurements are similar for both locations (1.79°C and 1.84°C), same as with relative humidity (20.86% and 21.00% respectively). The standard deviation of absolute humidity observations is lower in Wrocław than in Borowa Góra (0.63°C and 0.92°C, respectively).

Table 3. Statistics of temperature (T), absolute humidity (AH), and relative humidity (RH) residuals between radiometers' and radiosondes' measurements for Wrocław and Borowa Góra

		T [°C]	AH [g m^{-3}]	RH [%]
bias	WROC	–0.41	0.09	3.24
	BOGI	–0.17	0.21	3.60
standard deviation	WROC	1.79	0.63	20.86
	BOGI	1.84	0.92	21.00

Temperature and humidity profiles measured by RS and WVR were compared epoch by epoch, the results of two cases in Wrocław are presented in Figure 3. In the first case (January 30, 2021, 12:00, Fig. 3a) CBH was more than 10 km and the RS profiles of T and AH were smooth, no inversions in the vertical profiles were observed. The ra-

diometer's measurements present similar characteristics to RS data, the discrepancies between the two techniques are not larger than 1°C in T and 0.2 g m^{-3} in AH for the lower and middle troposphere (below 5 km). In the upper parts, larger differences in T are observed (up to 5°C for the altitudes higher than 5 km). The RH profile derived by radiosonde is much sharper than T and AH, with inversions at about 1, 4, and 8.5 km. In the radiometer's profile of RH, the large inversions in the upper troposphere are not noticed, however, the lower troposphere presents similarly to the RS data and the inversion is detected. Also, the shapes of the RH profiles are similar for the two data sources, but more smooth for WVR. In the second example (February 14, 2021, 00:00, Fig. 3b) CBH was low (about 1 km) and noticeable inversions in the profiles of AH and RH were detected by the radiosonde measurement. Also, slight temperature inversion was observed for the altitude of 1 km. In this case, radiometer's data do not reflect the state of the troposphere in the same way as the RS measurements; the radiometer's profiles of T, AH, and RH are smooth in the whole troposphere; for the two data sets, discrepancies of T, AH, and RH profiles reach 5°C, 2 g m^{-3} and 60%, respectively.

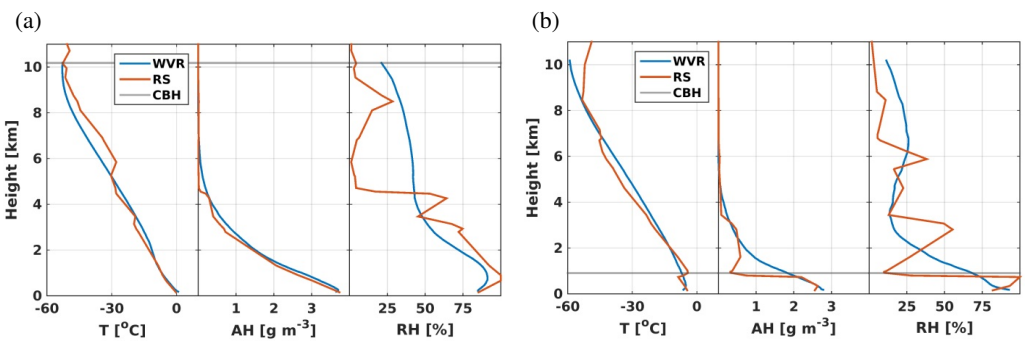

Fig. 3. Vertical profiles of temperature (T), absolute humidity (AH), and relative humidity (RH) in troposphere, derived from the microwave radiometers' measurements (WVR) and the radiosonde stations (RS) in Wrocław for January 30, 2021, 12:00 (a) and February 14, 2020, 00:00 (b). The horizontal grey lines denote cloud base height (CBH) measured by the microwave radiometer

The residuals between radiometers' and radiosonde's measurements of T, AH, and RH in the vertical profiles, for the entire period, are presented in Figure 4. Temperature's discrepancies between two measurement methods are in the range of –2°C to 2°C, with picks up to –5°C and 5°C in the higher parts of the troposphere (500–600 hPa). In the lower troposphere (900–800 hPa) temperatures measured by radiometers are larger than those of radiosondes, whereas in the upper troposphere (600-500 hPa) opposite results are noticed. In the location of Wrocław (Fig. 4a) residuals of temperature in the middle troposphere are negative for the period from September 2020 to February 2021 and positive in other cases. In Borowa Góra (Fig. 4b) the period of negative residuals of temperature in the middle troposphere is from January to April 2021. The discrepancies of absolute humidity are in the range of –2 g m^{-3} to 2 g m^{-3} and they are generally negative in the lower troposphere and positive in the upper troposphere. The exception is a period starting from February 2021 in Borowa Góra, where the radiometer's measurements of

AH below 800 hPa are larger than those of radiosonde by more than 1–2 g m^{-3}. The measurements of RH differ for the two techniques by about 30%. In the lower troposphere, the radiometers observe smaller values of RH than radiosondes, whereas in the upper troposphere (above 850 hPa) the residuals are mostly positive.

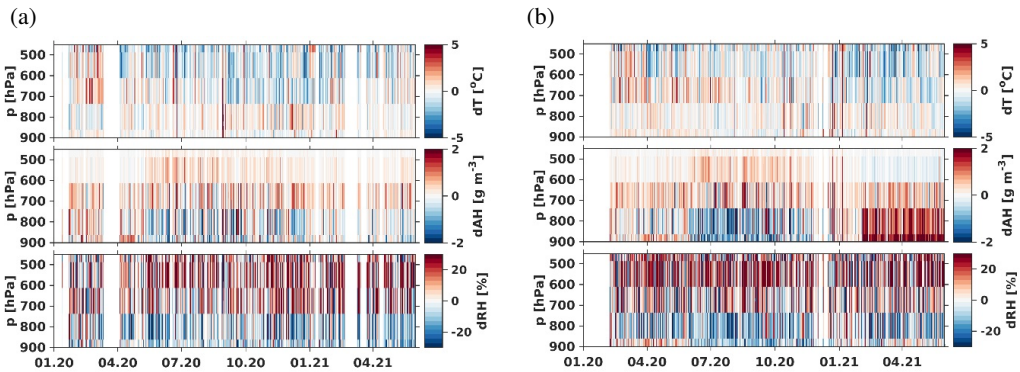

Fig. 4. Residuals of temperature (T), absolute humidity (AH), and relative humidity (RH) for radiometers' minus radiosondes' observations, presented in time (horizontal axis) and vertical levels (vertical axis). The left panel (a) refers to Wrocław, the right panel (b) refers to Borowa Góra

4.2. Meteorological parameters – comparison between radiometers, radiosondes and WRF model

The meteorological parameters were compared between 3 data sets for each pressure level separately, taking into account information about heavy rain events. The statistics of bias and standard deviation of temperature in two locations (Wrocław, Borowa Góra) for pressure levels up to 500 hPa (about 6 km) are presented in Figure 5. In the lower troposphere (below 800 hPa), a bias of temperature is the lowest when the microwave radiometer and radiosonde data (WVR RS, blue lines) are compared (0.2°C), whereas for the comparisons of radiometer – WRF (WVR WRF, red lines) and WRF – radiosonde (WRF RS, green lines) the bias is slightly larger in Wrocław (by about 0.1°C) and noticeably larger in Borowa Góra (by about 0.6°C). In general, the temperature's bias is negative for the comparison of WRF vs. RS and positive in other cases; it means that the values of T measured by the radiometer are overestimated when compared to RS and WRF, and the WRF model is underestimated when compared to RS. The statistics for the epochs with rainy events are presented using light shades. It is noticed that bias of temperature increases in rainy conditions, for all presented comparisons (by about 0.1°C in the lower troposphere in Wrocław and more than 2°C in the middle troposphere in Borowa Góra). The standard deviation of temperature in the lower troposphere (below 800 hPa) is the lowest for the radiometer vs. radiosonde comparison and is in the range of 0.8–1.5°C. For the other comparisons (WVR WRF and WRF RS) the values of standard deviation are larger by about 0.5°C in Wrocław and 0.8°C in Borowa Góra. In the middle troposphere (above 700 hPa) similar characteristics are noticed in Borowa Góra,

whereas in Wrocław the WRF RS comparison gives better results. Also, the rain impact on the standard deviation is more visible in the location of Borowa Góra (increase by more than 1°C in the lowest layer) than in Wrocław (decrease by about 0.5°C in the lowest layer).

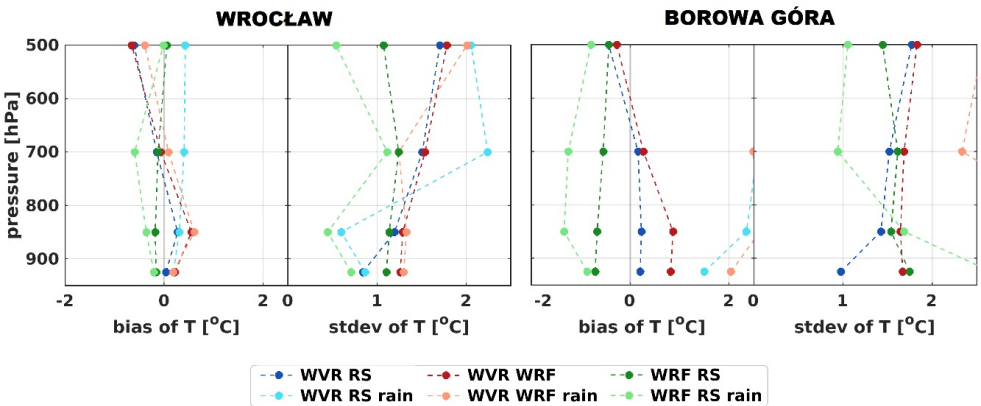

Fig. 5. Bias and standard deviation of temperature's (T) residuals at 4 pressure levels for microwave radiometer (WVR), radiosonde measurements (RS), and WRF model, calculated for all epochs and for rainy events only. Two locations are presented, Wrocław and Borowa Góra

The bias of absolute humidity is in a range of –0.5 g m^{-3} to 0.8 g m^{-3} for the typical meteorological conditions (without heavy rain) (Fig. 6). The best consistency is noticed for the WRF RS comparison (not more than 0.5 g m^{-3}). While the WVR RS and WVR WRF are compared, the AH bias values are negative in the lower layers in Wrocław and positive in other cases (above 700 hPa in Wrocław and for the whole profile in Borowa Góra). An impact of rain on the systematic error can be noticed in each case, especially

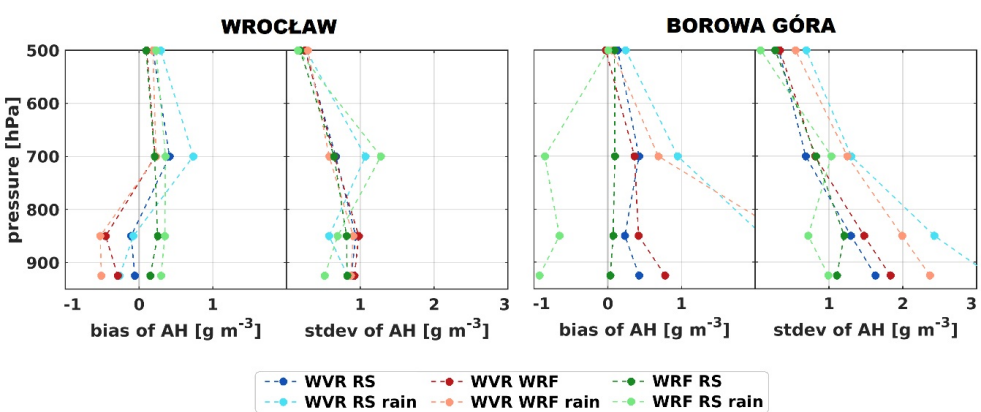

Fig. 6. Bias and standard deviation of absolute humidity (AH) residuals at 4 pressure levels for microwave radiometer (WVR), radiosonde measurements (RS), and WRF model, calculated for all epochs and for rainy events only. Two locations are presented, Wrocław and Borowa Góra

in the lower troposphere where the humidity is much higher (an increase of bias by 0.2 g m^{-3} in Wrocław and by more than 1 g m^{-3} in Borowa Góra). The standard deviation of absolute humidity in Wrocław is in the range of 0.5 g m^{-3} to 1.0 g m^{-3} with exception of rain events where the picks are up to 1.3 g m^{-3} in the middle troposphere (700 hPa) for the comparison between radiometer – radiosonde and WRF – radiosonde. In Borowa Góra, AH standard deviation is higher, in the range of 1.0–2.0 g m^{-3} in standard conditions and increases in rainy conditions by about 0.5 g m^{-3} in the whole profile for WVR RS and WVR WRF comparisons.

In terms of RH bias, the best consistency is noticed for the WRF RS comparison with values of –4% to 1%, whereas for the comparisons (WVR RS, WVR WRF) the bias reaches up to –9% in standard meteorological conditions (Fig. 7). During heavy rain events, the RH bias increases in the middle troposphere in Wrocław (by 5% for the WVR RS comparison) and in the lower troposphere in Borowa Góra (by more than 10% for the WRF RS comparison). The standard deviation of RH is in the range of 5–25% and it is not correlated to the heavy rain events.

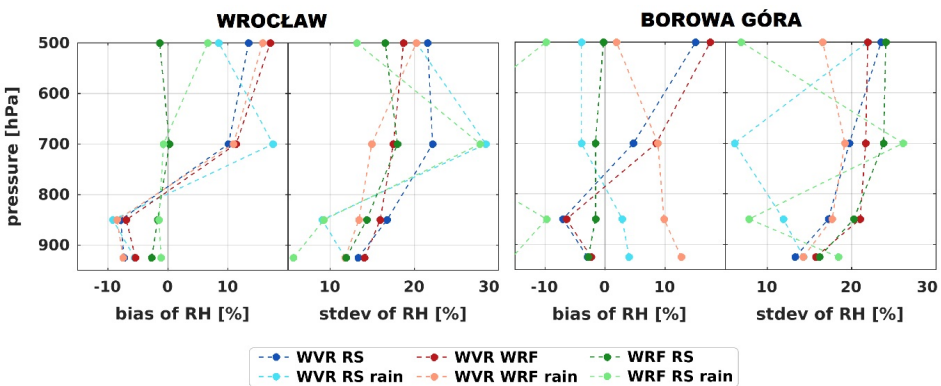

Fig. 7. Bias and standard deviation of relative humidity (RH) residuals at 4 pressure levels for microwave radiometer (WVR), radiosonde measurements (RS), and WRF model, calculated for all epochs and for rainy events only. Two locations are presented, Wrocław and Borowa Góra

5. Cross-comparison of ZTD products

5.1. Validation of the radiometers' ZTD measurements using radiosonde data

ZTD values from the microwave radiometer measurements were compared to the radiosonde observations, for the whole period, in two locations (Fig. 8). For better visibility, the plot presents the two data sets after the removal of bias between them. In both locations, ZTD values are in a range from 2.26 m in the winter months up to 2.56 m in the summer period. In Wrocław (Fig. 8a) discrepancies between radiometer's and radiosonde's measurements are in general lower than 0.01 m with picks up to 0.04 m in the summer. The histogram of the residuals for Wrocław shows a normal distribution of the discrepancies between the two data sets. In Borowa Góra (Fig. 8b) the first half of

the period has similar characteristics as the data from Wrocław; in the second half, large picks of residuals can be noticed, up to 0.15 m in January 2021. Also, after February 2021 radiometer's data are noticeably shifted up in reference to the radiosonde's data. This positive shift starts at the time when calibration of the radiometer in Borowa Góra took place (February 2, 2021). Due to different characteristics of the residuals in these two periods (before and after the calibration), two histograms are presented (each referring to one period). Before the calibration, the histogram is slightly shifted to the left side (by about 0.01 m), whereas after the calibration the shift is positive and more explicit (about 0.02 m).

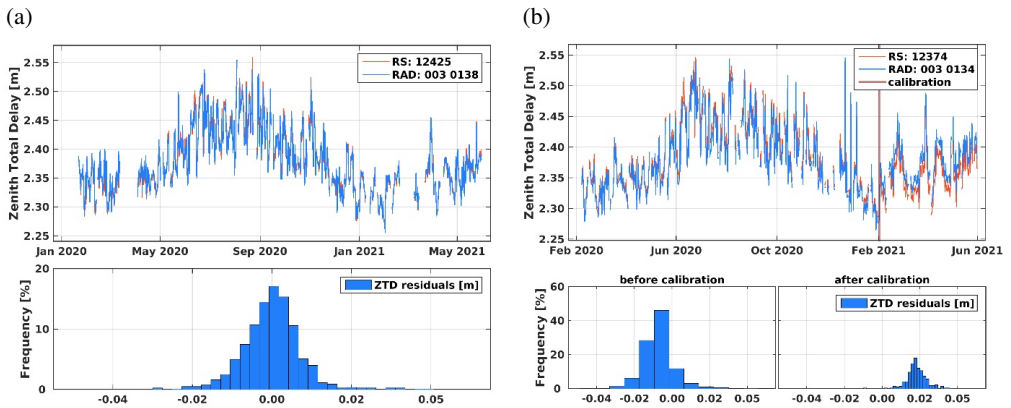

Fig. 8. ZTD time series of the radiometers' and radiosondes' observations (upper panels), together with the histograms of the residuals(lower panels). Two locations are presented, i. e. Wrocław (a) and Borowa Góra (b)

The statistics of bias and standard deviation for the radiometers' and radiosondes' residuals of ZTD observations were calculated for the two locations (Table 4). In Wrocław, a slight negative systematic error is noticed (radiometer's data underestimated) and equals –0.4 mm, whereas the standard deviation reaches 7.4 mm. In Borowa Góra, the radiometer's data are underestimated before February 2, 2021 (–5.7 mm) and noticeably overestimated in the second period (19.0 mm). The residuals of ZTDs in Borowa Góra have a larger standard deviation than those in Wrocław for the first period (13.9 mm) but it clearly decreased after the radiometer's calibration (5.4 mm).

Table 4. Statistics of ZTD residuals between radiometers' and radiosondes' measurements for Wrocław (WROC) and Borowa Góra (BOGI). The 2 periods refer to epochs before (period 1) and after (period 2) calibration of the radiometer in Borowa Góra (February 2, 2021). The column 'total' refers to the two periods together (before and after calibration of the radiometer in Borowa Góra)

	WROC	BOGI		
		total	period 1	period 2
ZTD bias [mm]	–0.4	0.8	–5.7	19.0
ZTD standard deviation [mm]	7.4	16.4	13.9	5.4

5.2. Validation of GNSS ZTD estimations with radiometers' and radiosondes' measurements as a reference

The ZTD values from the 3 GNSS solutions (EPN, PP, NRT) were validated against microwave radiometers' and radiosondes' measurements. Also, the WRF model was included in the comparisons. The systematic errors of the ZTD residuals for each solution in both locations (Wrocław, Borowa Góra) are presented in Figure 9. The ZTD statistics are calculated for the entire period in Wrocław and separated to 2 periods for the radiometer in Borowa Góra (before and after calibration of the instrument on February 2, 2021; both periods are referred to as BOGI-1 and BOGI-2). The largest values of ZTD bias are noticed for the radiometer in the case of BOGI-2, in the comparison to each data set, which shows the connection to the shifted values of ZTDs in Borowa Góra after the calibration on February 2, 2020. Also, the WRF model is characterized by large systematic error, exceeding –15.0 mm in Wrocław for both WVR and RS as a reference. The GNSS solutions (green, light green, yellow) are more consistent with the reference data in Borowa Góra (BOGI-1) than in Wrocław, for both reference cases (radiometers and radiosondes). In Wrocław, when the GNSS data are compared to the radiometers' measurements, the ZTD bias is in the range of –7.0 mm to –9.0 mm; similar results are found with the comparison to the radiosonde data. In Borowa Góra, when the first period is considered, better consistency is found between GNSS-radiometer data (0.5 mm to 3.0 mm) than GNSS-radiosonde data (–3.0 mm to –5.0 mm).

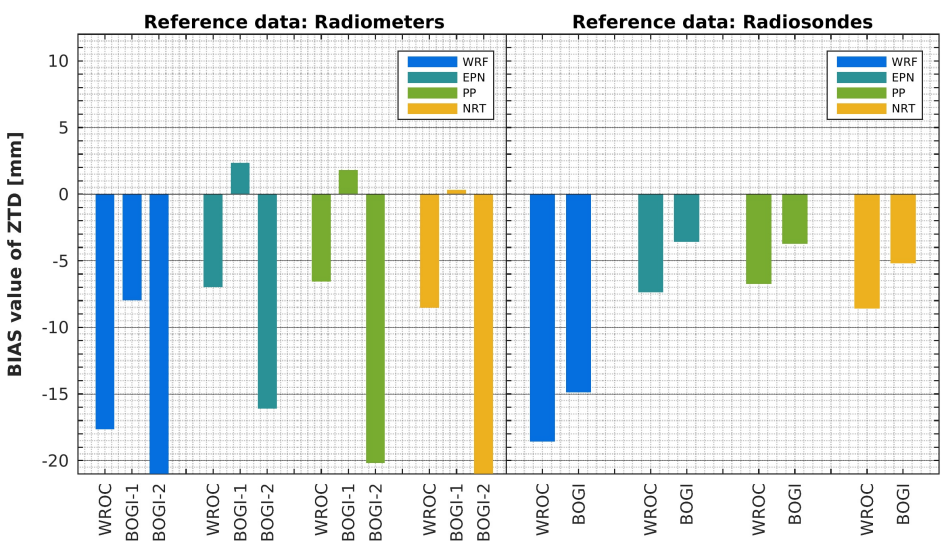

Fig. 9. Bias of ZTD residuals for the 6 data sets, with the radiometers' measurements (left panel) and the radiosonde's measurements(right panel) used as a reference. WRF stands for the WRF model; EPN, PP, and NRT stand for the GNSS-based solutions

In terms of standard deviation, the largest errors are noticed for the radiometer's data from Borowa Góra before calibration (BOGI-1) when compared to all other data sets

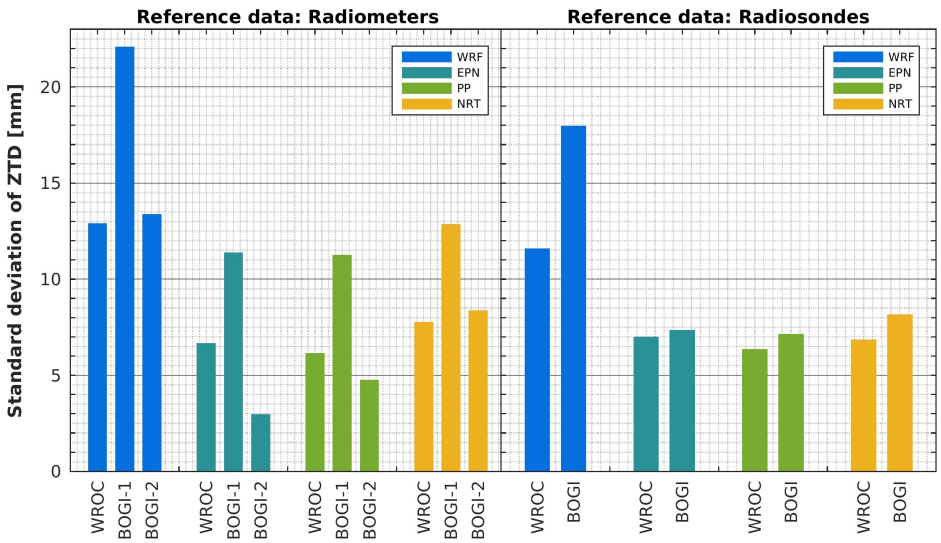

Fig. 10. Standard deviation of ZTD residuals for the 6 data sets, with the radiometers' measurements (left panel) and the radiosonde's measurements (right panel) used as a reference. WRF stands for the WRF model; EPN, PP, and NRT stand for the GNSS-based solutions

(in the range of 11–24 mm). Also, the WRF model is characterized by a large standard deviation (more than 12 mm with reference to both radiometers' and radiosondes' data). In Wrocław, the comparison between the GNSS and radiometer's measurements gives similar results as the comparison between the GNSS and radiosonde data (in range of 7.0–9.0 mm in terms of standard deviation). In Borowa Góra, EPN and PP solutions are more consistent with radiometers than with radiosondes by about 3.0–5.0 mm, whereas the NRT solution has a standard deviation of 8.0 mm for both reference data (radiometer and radiosonde).

6. Conclusions

In this study, the WVR measurements of temperature, humidity, and ZTD were compared to RS observations, the WRF model, and GNSS estimates. It was found that profiles of T and AH reflect a state of the troposphere similarly to the RS observations, especially in calm weather conditions (bias less than –0.5°C and 0.2 g m^{-3}, standard deviation less than 2°C and 1 g m^{-3}). The results are consistent with those given in the literature, where accuracy of the WVR temperature measurement is in range of 0.5–1.7°C for levels below 4 km (Crewell and Lohnert, 2007; Löhnert and Maier, 2012) and AH measurement accuracy is 0.15 g m^{-3} in terms of bias and 0.75 g m^{-3} in terms of standard deviation (Löhnert et al., 2009). The obtained results, point out that the WVR are well posed to be complementary profiling technique to GNSS tomography. The former have better performance in the bottom part of the atmosphere especially in the boundary layer

(Crewell and Lohnert, 2007), while the latter may achieve more stable profiles above 2km (1 g m^{-3} of STD with almost no bias) (Brenot et al., 2020). Profiles of relative humidity show a larger discrepancy between the WVR and RS measurements (residuals up to 60%). The largest discrepancies between WVR and RS observations of temperature and humidity can be noticed for the epochs with low cloud base height (about 1 km), as well as for heavy precipitation events (an increase of T bias by 0.5°C and AH bias and standard deviation by more than 2 g m^{-3}, in the lower and middle troposphere). The low accuracy of measurement during rainy events is in line with the expectations, since the WVR technique is not recommended for the high-precipitation conditions (Löhnert et al., 2009; Massaro et al., 2015). In the case of temperature observations, a similar agreement is noticed for all three data sources (WVR, RS, WRF model), whereas for humidity the best agreement between RS and WRF was found.

In terms of ZTD, the comparison of WVR and RS techniques results in bias equal to –0.4 mm and a standard deviation of 7.4 mm in Wrocław. The values obtained are consistent with the literature, where the agreement between RS and WVR is on the level of 1–2 mm in terms of PWV, which is 6–12 mm in terms of ZWD (Rocken et al. 1995; Emardson et al. 2000). In Borowa Góra, issues due to the instrument's calibrations might disturb the real level of agreement between the techniques. In both cases (Wrocław and Borowa Góra), the largest discrepancies were found during the summer period (an increase of ZTD residuals from 10 mm in winter up to 40 mm in summer). This increase of the discrepancies might result of a higher variability of humidity in the troposphere in the summer months, which has a negative impact on the GNSS ZTD estimations (Haase et al., 2003). The GNSS data verification using two data sources (WVR, RS) shows similar results in most cases, i.e., bias and standard deviations at a level of 7.0–9.0 mm which is consistent with the literature (Rocken et al. 1995; Emardson et al. 2000). Better agreement between GNSS and WVR than GNSS and RS was noticed in Borowa Góra, in terms of bias before the calibration (by 5.0 mm for the NRT solution) and in terms of standard deviation after the calibration (by 3.0 mm for the EPN solution).

The presented study shows the potential of the WVR technique as an additional data source for the GNSS tropospheric products validation. Further works should be focused on testing this technique during different weather conditions, to get more detailed characteristics of the measurements accuracy e.g. depending on cloud base heights. Also, slant WVR observations of tropospheric delay could be verified as a possible data source for the GNSS troposphere tomography or NWP models.

Author contributions

Conceptualization: E.T., D.T., and W.R.; conceived and planned the experiments: E.T., D.T., and W.R.; carried out the experiments and contributed to preparing the figures: E.T. and D.T.; contributed to the interpretation of the results: E.T. and W.R.; took the lead in writing the manuscript with input from all authors: E.T.; provided critical feedback and helped shape the research, analysis and manuscript: E.T, D.T., and W.R.

Data availability statement

The datasets of water vapour radiometer observations analysed during the current study are available from the corresponding author on a request. The radiosonde observations are available at the University of Wyoming website (http://weather.uwyo.edu/upperair/sounding.html). The WRF model data were provided by the Department of Climatology and Atmosphere Protection (http://www.meteo.uni.wroc.pl/) at the University of Wroclaw and are available from the corresponding author on a reasonable request.

Acknowledgements

This research was part of the project EPOS-PL, European Plate Observing System POIR.04.02.00–14-A003/16. The authors gratefully acknowledge the Wrocław Center of Networking and Supercomputing (http://www.wcss.wroc.pl/) computational grant using MATLAB Software License No. 101979 and computational Grant No. 170.

References

Bauer, H.-S., Wulfmeyer, V., Schwitalla, T. et al. (2011). Operational assimilation of GPS slant path delay measurements into the MM5 4DVAR system. Tellus A: *Dynamic Meteorology and Oceanography*, 63, 263–282. DOI: 10.1111/j.1600-0870.2010.00489.x.

Bengtsson, L. (2010). The global atmospheric water cycle. *Environ. Res. Lett.*, 5, 202. DOI: 10.1088/1748-9326/5/2/025202.

Bennitt, G.V. and Jupp, A. (2012). Operational assimilation of GPS zenith total delay observations into the Met Office numerical weather prediction models. *Mon. Weather Rev*., 140, 2706–2719. DOI: 10.1175/MWR-D-11-00156.1.

Bevis, M., Businger, S., Chiswell, T.A. et al. (1994). Gps meteorology: Mapping zenith wet delays onto precipitable water. *J. Appl. Meteorol. Climatol*., 33 (3), 379–386. DOI: 10.1175/1520-0450(1994)033<0379:GMMZWD>2.0.CO;2.

Bock, O., Bosser, P., Pacione, R. et al. (2016). A high-quality reprocessed ground-based GPS dataset for atmospheric process studies, radiosonde and model evaluation, and reanalysis of HyMeX S pecial Observing Period. *Q. J. R. Meteorol. Soc.*, 142, 56–71. DOI: 10.1002/qj.2701.

Böhm, J. and Schuh, H. (2013). *Atmospheric effects in space geodesy*. Springer. DOI: 10.1007/978-3-642-36932-2S.

Boniface, K., Ducrocq, V., Jaubert, G. et al. (2009). Impact of high-resolution data assimilation of GPS zenith delay on Mediterranean heavy rainfall forecasting. *Ann. Geophys.*, 27, 2739–2753. DOI: 10.5194/angeo-27-2739-2009.

Brenot, H., Rohm, W., Kačmařík, M. et al. (2020). Cross-Comparison and methodological improvement in GPS tomography. *Remote Sens.*, 12(1), 30. DOI: 10.3390/rs12010030.

Buehler, S., Östman, S., Melsheimer, C. et al. (2012). A multi-instrument comparison of integrated water vapour measurements at a high latitude site. *Atmospheric Chem. Phys.*, 12, 10925–10943. DOI: 10.1.1.662.8109.

Churnside, J.H., Stermitz, T.A., and Schroeder, J.A. (1994). Temperature Profiling with Neural Network Inversion of Microwave Radiometer Data. *J. Atmos. Ocean Technol.*, 11(1).

Crewell, S., and Lohnert, U. (2007). Accuracy of boundary layer temperature profiles retrieved with multifrequency multiangle microwave radiometry. *IEEE Trans.Geosci.Remote Sens.*, 45(7), 2195–2201. DOI: 10.1109/TGRS.2006.888434.

Dach, R., Lutz, S., Walser, P. et al. (2015). *Bernese GNSS Software Version 5.2. User manual, Astronomical Institute*. Universtiy of Bern: Bern Open Publishing.

Dai, A., Wang, J., Ware, R.H. et al. (2002). Diurnal variation in water vapor over North America and its implications for sampling errors in radiosonde humidity. *J. Geophys. Ress: Atmos.,* 107, ACL-11. DOI: 10.1029/2001JD000642.

Dymarska, N., Rohm, W., Sierny, J. et al. (2017). An assessment of the quality of near-real time GNSS observations as a potential data source for meteorology. *Meteorol. Hydro. Water Managem. Res. Operational Applications*, 5, 3–13. DOI: 10.26491/mhwm/65146.

Emardson, T.R., Johansson J.M., and Elgered G. (2000). The systematic behavior of water vapor estimates using four years of GPS observations. *IEEE Trans. Geosci. Remote Sens.*, 38, 324–329. DOI: 10.1109/36.823927.

Ferraro, R.R., Kusselson, S.J., and Colton, M. (1998). An introduction to passive microwave remote sensing and its applications to meteorological analysis and forecasting. *Polarization*, 1(2). DOI: 10.1.1.662.8109.

Ferreira, J.A., Liberato, M.L., and Ramos, A.M. (2016). On the relationship between atmospheric water vapour transport and extra-tropical cyclones development. *Phys. Chemis. Earth*, Parts A/B/C, 94, 56–65. DOI: 10.1016/j.pce.2016.01.001.

Frate, F.D. and Schiavon, G. (1998). A combined natural orthogonal functions/neural network technique for the radiometric estimation of atmospheric profiles. *Radio Sci.*, 33, 405–410. DOI: 10.1029/97RS02219.

Gradinarsky, L., Johansson, J., Bouma, H. et al. (2002). Climate monitoring using GPS. *Phys. Chemis. Earth*, Parts A/B/C, 27, 335–340. DOI: 10.1016/S1474-7065(02)00009-8.

Guerova, G., Brockmann, E., Schubiger, F. et al. (2005). An integrated assessment of measured and modeled integrated water vapor in Switzerland for the period 2001-03. *J. Appl. Meteorol. Climatol.*, 44, 1033–1044. DOI: 10.1175/JAM2255.1.

Guerova, G., Jones, J., Douša, J. et al. (2016). Review of the state of the art and future prospects of the ground-based GNSS meteorology in Europe. *Atmos. Meas. Tech.*, 9, 5385–5406. DOI: 10.5194/amt-9-5385-2016.

Haase, J., Ge, M., Vedel, H. et al. (2003). Accuracy and variability of GPS tropospheric delay measurements of water vapor in the western Mediterranean. *J. Appl. Meteorol.*, 42(11), 1547–1568. DOI: 10.1175/1520-0450(2003)042<1547:AAVOGT>2.0.CO;2.

Hanna, N., Trzcina, E., Möller, G. et al. (2019). Assimilation of GNSS tomography products into WRF using radio occultation data assimilation operator. *Atmos. Meas.Tech.s Discuss.*, 1–32. DOI: 10.5194/amt-12-4829-2019.

Ingram, W. (2010). A very simple model for the water vapour feedback on climate change. *Quarterly J. R. Meteorol. Soc.*, 136, 30–40. DOI: 10.1002/qj.546.

Jacob, D. (2001). The role of water vapour in the atmosphere. A short overview from a climate modeller's point of view. *Physics and Chemistry of the Earth, Part A: Solid Earth and Geodesy*, 26, 523–527. DOI: 10.1016/S1464-1895(01)00094-1.

Jung, T., Ruprecht, E., and Wagner, F. (1998). Determination of cloud liquid water path over the oceans from Special Sensor Microwave/Imager (SSM/I) data using neural networks. *J. Appl. Meteorol.*, 37, 832–844. DOI: 10.1175/1520-0450(1998)037<0832:DOCLWP>2.0.CO;2.

Karabatić, A., Weber, R., and Haiden, T. (2011). Near real-time estimation of tropospheric water vapour content from ground based GNSS data and its potential contribution to weather now-casting in Austria. *Adv. Space Res.*, 47, 1691–1703. DOI: 10.1016/j.asr.2010.10.028.

Kleijer, F. (2004). *Troposphere modeling and filtering for precise GPS leveling*. Ph.D. thesis. TU Delft: Delft University of Technology. DOI: 10.26491/mhwm/65146.

Kryza, M., Werner, M., Wałszek, K. et al. (2013). Application and evaluation of the WRF model for high-resolution forecasting of rainfall-a case study of SW Poland. *Meteorologische Zeitschrift*, 22, 595–601. DOI: 10.1127/0941-2948/2013/0444.

Liang, H., Cao, Y., Wan, X. et al. (2015). Meteorological applications of precipitable water vapor measurements retrieved by the national GNSS network of China. *Geod. Geodyn.*, 6, 135–142. DOI: 10.1016/J.GEOG.2015.03.001.

Liou, Y.-A., Teng, Y.-T., Van Hove, T. et al. (2001). Comparison of precipitable water observations in the near tropics by GPS, microwave radiometer, and radiosondes. *J. Appl. Meteorol.*, 40, 5–15. DOI: 10.1175/1520-0450(2001)040<0005:COPWOI>2.0.CO;2.

Liu, J., Sun, Z., Liang, H. et al. (2005). Precipitable water vapor on the Tibetan Plateau estimated by GPS, water vapor radiometer, radiosonde, and numerical weather prediction analysis and its impact on the radiation budget. *J. Geophys. Res. Atmos.*, 110. DOI: 10.1029/2004JD005715.

Löhnert, U., Turner, D.D., and Crewell, S. (2009). Ground-Based Temperature and Humidity Profiling Using Spectral Infrared and Microwave Observations. Part I: Simulated Retrieval Performance in Clear-Sky Conditions. *J. Appl. Meteorol. Climatol.*, 48(5), 1017–1032. DOI: 10.1175/2008JAMC2060.1.

Löhnert, U., and Maier, O. (2012). Operational profiling of temperature using ground-based microwave radiometry at Payerne: Prospects and challenges. *Atmos. Meas. Tech.*, 5(5), 1121–1134. DOI: 10.5194/amt-5-1121-2012.

Lu, C., Li, X., Li, Z. et al. (2016). GNSS tropospheric gradients with high temporal resolution and their effect on precise positioning. *J. Geophys. Res. Atmos.*, 121, 912–930. DOI: 10.1002/2015JD024255.

Mahfouf, J.-F., Ahmed, F., Moll, P. et al. (2015). Assimilation of zenith total delays in the AROME France convective scale model: a recent assessment. *Tellus A: Dyn. Meteorol. Oceanogr.*, 67, 26106. DOI: 10.3402/tellusa.v67.26106.

Massaro, G., Stiperski, I., Pospichal, B. et al. (2015). Accuracy of retrieving temperature and humidity profiles by ground-based microwave radiometry in truly complex terrain. *Atmos. Meas. Tech.*, 8(8), 3355–3367. DOI: 10.5194/amt-8-3355-2015.

Miloshevich, L.M., Paukkunen, A., Vömel, H. et al. (2004). Development and validation of a time-lag correction for Vaisala radiosonde humidity measurements. *J. Atmos. Oceanic Tech.*, 21, 1305–1327. DOI: 10.1175/1520-0426(2004)021<1305:DAVOAT>2.0.CO;2.

Möller, G., Wittmann, C., Yan, X. et al. (2015). *3D ground based GNSS atmospheric tomography*. Final report, FFG project GNSS-ATom (ID:840098).

Morland, J., Collaud Coen, M., Hocke, K. et al. (2009). Tropospheric water vapour above Switzerland over the last 12 years. *Atmos. Chemis. Phys.*, 9, 5975–5988, 2009. DOI: 10.5194/acp-9-5975-2009.

Ning, T. and Elgered, G. (2021). High temporal resolution wet delay gradients estimated from multi-GNSS and microwave radiometer observations. *Atmos. Meas. Tech. Discuss.*, 1–21. DOI: 10.5194/amt-14-5593-2021.

Offiler, D. (2010). EIG EUMETNET GNSSWater Vapour Programme (E-GVAP-II) Product Requirements Document. Tech. rep. EIG EUMETNET.

Ohtani, R. and Naito, I. (2000). Comparisons of GPS-derived precipitable water vapors with radiosonde observations in Japan. *J. Geophys. Res. Atmos.*, 105, 26917–26929. DOI: 10.1029/2000JD900362.

Pacione, R., Pace, B., Vedel, H. et al. (2011). Combination methods of tropospheric time series. *Adv. Space Res*. DOI: 10.1016/j.asr.2010.07.021.

Pacione, R., Araszkiewicz, A., Brockmann, E. et al. (2017). EPN-Repro2: A reference GNSS tropospheric data set over Europe. *Atmos. Meas. Tech.*, 10, 1689–1705. DOI: 10.5194/amt-10-1689-2017.

Rocken, C., Van Hove, T., Johnson et al. (1995). GPS/STORM–GPS sensing of atmospheric water vapor for meteorology. *J. Atmos. Oceanic Technol*., 12, 468–478. DOI: 10.1175/1520-0426(1995)012<0468:GSOAWV>2.0.CO;2.

Rohm, W., Guzikowski, J., Wilgan, K. et al. (2019). 4DVAR assimilation of GNSS zenith path delays and precipitable water into a numerical weather prediction model WRF. *Atmos. Meas.Tech.*, 12, 345–361. DOI: 10.5194/amt-12-345-2019.

RPG: Operation Principles and Software Description for RPG standard single polarization radiometers (G5series), Radiometer Physics GmbH, Werner-von-Siemens-Str. 4, 53340 Meckenheim, Germany, 12 edn., https://www.radiometer-physics.de, 2017.

Sá, A., Rohm, W., Fernandes, R.M. et al. (2021). Approach to leveraging real-time GNSS tomography usage. *J. Geod.*, 95(1), 1–21. DOI: 10.1007/s00190-020-01464-7.

Shangguan, M., Heise, S., Bender, M. et al. (2015). Validation of GPS atmospheric water vapor with WVR data in satellite tracking mode. *Annal. Geophys.*, 33, 55–61. DOI: 10.5194/angeo-33-55-2015.

Skamarock, W.C., Klemp, J.B., Dudhia, J. et al. (2008). *A description of the Advanced Research WRF version 3*. NCAR Technical note-475+ STR. DOI: 10.5065/D68S4MVH.

Solheim, F., Godwin, J.R., Westwater, E. et al. (1998). Radiometric profiling of temperature, water vapor and cloud liquid water using various inversion methods. *Radio Sci.*, 33, 393–404. DOI: 10.1029/97RS03656.

Thayer, G.D. (1974). An improved equation for the radio refractive index of air. *Radio Sci.*, 9, 803–807. DOI: 10.1029/RS009i010p00803.

Tondaś, D., Kapłon, J., and Rohm, W. (2020). Ultra-fast near real-time estimation of troposphere parameters and coordinates from GPS data. *Measurement*, 107849. DOI: 10.1016/j.measurement.2020.107849.

Trzcina, E. and Rohm,W. (2019). Estimation of 3D wet refractivity by tomography, combining GNSS and NWP data: First results from assimilation of wet refractivity into NWP. *Q. J. R. Meteorol. Soc.*, 145, 1034–1051. DOI: 10.1002/qj.3475.

Trzcina, E., Hanna, N., Kryza, M. et al. (2020). TOMOREF Operator for Assimilation of GNSS Tomography Wet Refractivity Fields in WRF DA System. *J. Geophys. Res. Atmos.*, 125, e2020JD032, 451. DOI: 10.1029/2020JD032451.

Ulaby, F., Moore, R., and Fung, A. (1986). *An improved equation for the radio refractive index of air*. Artech House, I–II. DOI: 10.1029/RS009i010p00803.

Van Baelen, J., Aubagnac, J.-P., and Dabas, A. (2005). Comparison of near–real time estimates of integrated water vapor derived with GPS, radiosondes, and microwave radiometer. *J. Atmos. Oceanic Tech.*, 22, 201–210. DOI: 10.1175/JTECH-1697.1.

Van Baelen, J., Reverdy, M., Tridon, F. et al. (2011). On the relationship between water vapour field evolution and the life cycle of precipitation systems. *Q. J. R. Meteorol. Soc.*, 137, 204–223. DOI: 10.1002/qj.785.

Vey, S., Dietrich, R., Rülke, A. et al. (2010). Validation of precipitable water vapor within the NCEP/DOE reanalysis using global GPS observations from one decade. *J. Clim.*, 23, 1675–1695. DOI: 10.1175/2009JCLI2787.1.

Wang, J. and Liu, Z. (2019). Improving GNSS PPP accuracy through WVR PWV augmentation. *J. Geod.*, 93, 1685–1705. DOI: 10.1007/s00190-019-01278-2.

Wilgan, K., Rohm, W., and Bosy, J. (2015). Multi-observation meteorological and GNSS data comparison with Numerical Weather Prediction model. *Atmos. Res.*, 156, 29–42. DOI: 10.1016/j.atmosres.2014.12.011.

Zhao, Q., Yao, Y., Yao, W. et al. (2019a). GNSS-derived PWV and comparison with radiosonde and ECMWF ERA-Interim data over mainland China. *J. Atmos. and Sol.-Terr. Phys.*, 182, 85–92. DOI: 10.1016/j.jastp.2018.11.004.

Zhao, Y., Xu, X., Zhao, T. et al. (2019b). Effects of the Tibetan Plateau and its second staircase terrain on rainstorms over North China: From the perspective of water vapour transport. *Intern. J. Climat.*, 39, 3121–3133. DOI: 10.1002/joc.6000.

Zus, F., Wickert, J., Bauer, H.S. et al. (2011). Experiments of GPS slant path data assimilation with an advanced MM5 4DVAR system. *Meteorologische Zeitschrift*, 173–184. DOI: 10.1127/0941-2948/2011/0232.